Ultraviolet Emission of ZnS Nanoparticles Confined within a Functionalized Mesoporous Host

Weon-Sik Chae,[†] Joong-Ho Yoon,[†] Hyunung Yu,[†] Du-Jeon Jang,[‡] and Yong-Rok Kim*[,†]

Department of Chemistry, Yonsei University, Seoul, 120-749, and School of Chemistry, Seoul National University, Seoul 151-742, South Korea

Received: April 15, 2004; In Final Form: May 25, 2004

A highly loaded ZnS nanoparticle (NP) array within mesoporous channels was prepared by repetitive insertion of ZnS reverse micelles. Contrary to the ZnS NPs in the water pool of reverse micelles exhibiting blue emission, the ZnS NPs incorporated within the organically functionalized mesoporous channels showed the emission in the ultraviolet region with a single recombination lifetime of 1.3 ± 0.2 ns. Such optical characteristics are considered to dominantly originate from the potential traps of lattice sulfur vacancies existing in the confined ZnS NPs within the fit size of the functionalized host pore channels.

1. Introduction

Highly ordered mesoporous materials have been utilized as templates for the preparation of nanomaterials with controlled dimension and morphology. By now, a number of studies have focused on the incorporation of various functional materials, such as metals,[1−4] semiconductors,[5−9] magneto-semiconductors,[10−12] and organic molecules,[13] within the mesoporous templates, by using several synthetic methods of wet chemical impregnation,[1,3,4,8,9,11,12] chemical vapor infiltration (CVI),[2] and metal−organic chemical vapor deposition (MOCVD).[5,6]

Although well-ordered arrays of nanostructures of nanoparticles (NPs) and nanowires are successfully accomplished within mesoporous templates, there are few studies on the energetic properties and the manipulation of the energetic properties. Most of the previous studies presented largely Stokes shifted broad emissions for the confined II−VI semiconductor (SC) NPs within mesoporous hosts,[14−16] which was generally responsible for the surface defect states of the SC NPs. Unfortunately, such energetic properties from the surface defect states are difficult to control due to complicated interactions with the environments. For the application aspects, however, control of energetic properties is highly demanded for the ordered SC NP arrays. Therefore, a proper preparation method should be applied for the modification of energetic properties of SC NP arrays.

Recently, confined CdS NPs within siliceous mesoporous channels opened a new possibility of modification of their energetic properties through organic functionalization of the mesoporous channels; a functionalized mesoporous host enabled suppression of undesired emission from the surface defect states.[17] In this study, the confined ZnS NPs within organically functionalized (HS−$CH_2CH_2CH_2$−Si≡) mesoporous MCM-41 (FM-41) channels presented only ultraviolet emission that arises solely from the core states rather than the surface states. And the recombination lifetime for this ultraviolet emission was found to be a single component of 1.3 ± 0.2 ns.

* To whom correspondence should be addressed. E-mail: yrkim@alchemy.yonsei.ac.kr.

[†] Yonsei University.

[‡] Seoul National University.

2. Experimental Section

2.1. Preparation. Water containing sodium bis(2-ethylhexyl) sulfosuccinate (AOT; Aldrich) reverse micelles in an oil phase were utilized, as nanoreactors, to prepare the ZnS NPs. For the preparation of H_2O/AOT/*n*-octane reverse micelles, a W_o ratio ([H_2O]/[AOT]) of 3 was selected, and preparation of the reverse micelles containing ZnS NPs was performed according to the previous study.[17]

The mesoporous FM-41 host was prepared by the following two-step process as reported in the literature:[17,18] a typical supramolecular templating method for the mesoporous MCM-41 host[4] and organic functionalization of the resulting mesoporous host by using tris(methoxy)(mercaptopropylsilane) ($HSCH_2CH_2CH_2Si(CH_3O)_3$) as an organic modification agent.

Insertion of the ZnS NP/AOT/*n*-octane reverse micelles into the nanochannels of the FM-41 host was performed as follows: 0.2 g of the FM-41 host was added to the ZnS NP/AOT/*n*-octane reverse micellar solution (20 mL) after formation of the ZnS NPs (ca. 5 min). The mixture was slowly stirred for 10 h for insertion of the ZnS reverse micelles into the FM-41 channels, followed by centrifugation and decantation (the first insertion). To increase the loading amount of the ZnS NPs within the FM-41 host, the resulting precipitate was resuspended into another ZnS reverse micellar solution (20 mL) and the resulting suspension slowly stirred for 10 h, followed by centrifugation and decantation (the second insertion). After insertion, the precipitate powders were resuspended in *n*-octane for 10 min to remove the ZnS NPs possibly existing on the outer surface of the host channels, and subsequently centrifuged. The final powder samples were dried overnight in an oven at 80 °C. The samples are denoted as ZnS@FM-1 and ZnS@FM-2 according to the number of repetitive insertions.

2.2. Characterization. The absorption spectrum was measured with a UV−vis spectrophotometer (Shimadzu, UV-160A). For the powder samples, diffuse reflectance spectra were recorded on a UV−vis spectrophotometer (Jasco, V-550) equipped with an integrating sphere (Jasco, ISV-469). X-ray diffraction data were obtained on a diffractometer (Mac Science M03XHF[22]) with copper radiation (λ = 1.54056 Å). Transmission electron microscopy (TEM) images were obtained with a microscope (JEOL, 3010) that was operated at 200 kV with

10.1021/jp048349m CCC: $27.50
Published on Web 07/01/2004

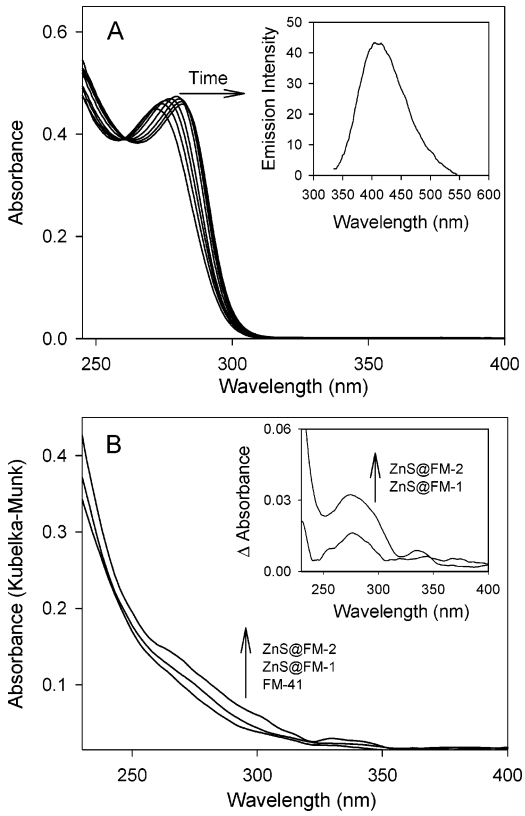

Figure 1. (A) Absorption spectra of the ZnS NPs in the reverse micelles ($W_o = 3$) for an observation period of 10 h: as-made, 10 min, 20 min, 30 min, 1 h, 2 h, and 10 h. The inset shows the emission spectrum of the ZnS NPs in the water pool of reverse micelles after 10 h. The excitation wavelength is 280 nm. (B) Absorption spectra for FM-41, ZnS@FM-1, and ZnS@FM-2. The inset shows the absorption spectra of the ZnS NPs which are obtained by subtracting the FM-41 host spectrum from the spectra of the nanocomposites including ZnS NPs. The absorption spectra of the nanocomposites were obtained by applying the Kubelka−Munk function to the diffuse reflectance spectrum.

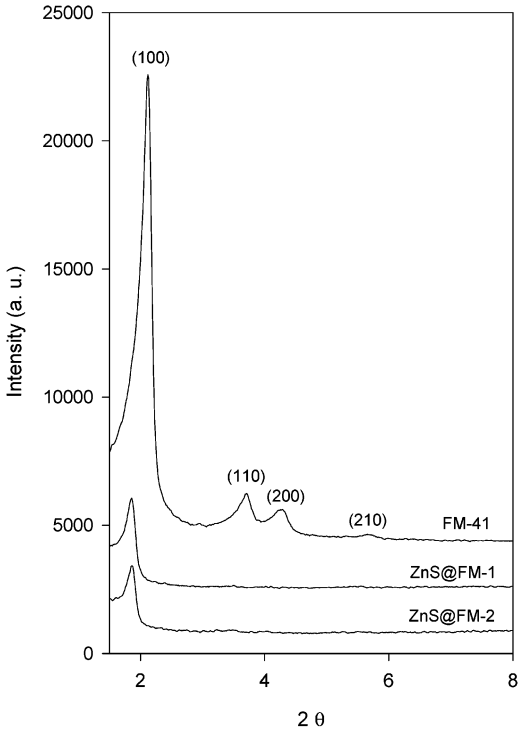

Figure 2. X-ray diffractions for FM-41, ZnS@FM-1, and ZnS@FM-2. Miller planes of the characteristic hexagonal structure are indicated for the mesoporous FM-41 host.

the sample deposited on a holey carbon copper grid. Nitrogen adsorption measurements were carried out by using an adsorption analyzer (Micromeritics, ASAP 2010). Before the measurements, the samples were degassed for 2 h at 473 K under a vacuum of $\sim 10^{-3}$ Torr. Photoluminescence (PL) and photoluminescence excitation (PLE) spectra were obtained by using a fluorescence spectrometer (Hitachi, F-4500), and time-resolved PL decays were measured by using a picosecond laser system consisting of an actively/passively mode-locked Nd:YAG laser (Quantel, YG501) and a 10 ps streak camera (Hamamatsu, C2830) attached to a CCD detector (Princeton Instruments, RTE128H). The instrumental response function (IRF) was 240 ps in full width at half-maximum (fwhm). Details of the laser system are described elsewhere.[19]

3. Results and Discussion

The structural confinement was accomplished by incorporation of ZnS NPs into the organically functionalized mesoporous MCM-41 host. Reverse micelles containing ZnS NPs were used as insertion carriers into the FM-41 host, similarly to those in our previous work of incorporation of CdS NPs within a mesoporous host.[17] As-made reverse micelles containing ZnS NPs show a sharp exciton absorption band around 273 nm (Figure 1A). On the basis of the previous experimental results and theoretical calculations,[20−22] it is estimated that the diameters of the as-made ZnS NPs are stably maintained at $\sim 2.0 \pm 0.2$ nm during the observed period of 10 h. The emission spectrum of the ZnS NPs in the water pool of reverse micelles shows largely Stokes shifted blue emission centered at 410 nm and expanded to 545 nm (inset of Figure 1A). It is generally suggested that the emission spectrum of 400−600 nm originates from the surface defect states such as sulfur vacancies located at the surface of ZnS NPs.[23,24]

To increase the loading amount of the ZnS NPs within the FM-41 host, insertion of the reverse micelles was repetitively performed. At the first loading of the ZnS NPs into the FM-41 host (ZnS@FM-1), an absorption shoulder appears around 275 nm in addition to the background absorption of the FM-41 host itself (Figure 1B). And the absorption shoulder is further enhanced as the insertion of the ZnS NPs into the FM-41 host is repeated one more time. The absorption difference between the ZnS NP loaded host and the empty FM-41 host clearly shows the enhancement of the exciton absorption with the increased loading amount (inset of Figure 1B).

Powder X-ray diffraction of the organically modified mesoporous host (FM-41) exhibits the characteristic pattern corresponding to a hexagonally ordered mesoporous structure (Figure 2). After incorporation of the ZnS NPs within the FM-41 host, the diffraction intensity of the (100) plane of the FM-41 host is highly reduced and the diffraction peak of the (100) plane is shifted to lower angle (from 2.12° to 1.86°) in both the ZnS@FM-1 and ZnS@FM-2 cases. The reduced intensity of the diffraction peak is ascribed to the incorporation of the ZnS NPs within the FM-41 host. Previous studies suggested that incorporation of guest NPs within mesoporous channels reduced the contrast between the wall framework and porous channel, which resulted in reduction of the diffraction intensity of the mesoporous host.[7,8,12] And the observed increase of the $d_{(100)}$ spacing (from 41.64 to 47.46 Å) of the FM-41 host is due to the widening of the mesoporous channels during the incorporation of the ZnS NPs into the FM-41 host. Similar pore widening

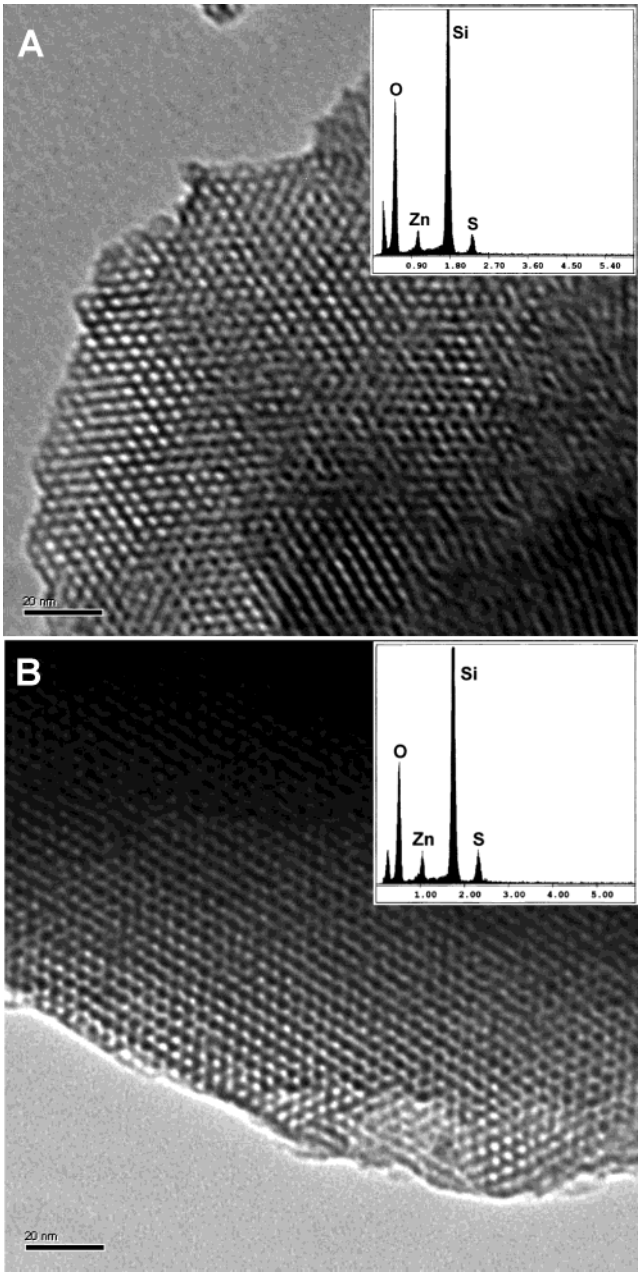

Figure 3. TEM images for (A) ZnS@FM-1 and (B) ZnS@FM-2 exhibiting a hexagonally arrayed structure. The insets are the EDX spectra of the corresponding nanocomposites including the impregnated ZnS NPs.

was previously observed during the inclusion chemistry of guest NPs into mesoporous silica materials.[6,9,15]

TEM images of the nanocomposite materials with ZnS NPs (ZnS@FM-1 and ZnS@FM-2) show long-range-ordered hexagonal arrays of the mesoporous FM-41 host (Figure 3), which confirm the conservation of the characteristic mesoporous structure of the FM-41 host after incorporation of the ZnS NPs. And no large external ZnS NPs are observed at the outside of the mesoporous FM-41 channels. X-ray energy dispersion (EDX) analysis indicates that the averaged loading contents of the ZnS NPs within the FM-41 host are 16.3 ± 1.0 and 21.1 ± 1.5 wt % for the respective ZnS@FM-1 and ZnS@FM-2. The elemental ratio is shown to be $1.0{:}0.55 \pm 0.05$ for Zn:S, which is similar to the elemental ratios observed for the small-sized II−VI semiconductors.[25,26]

The nitrogen adsorption isotherm often provides valuable information for guest incorporation within mesoporous

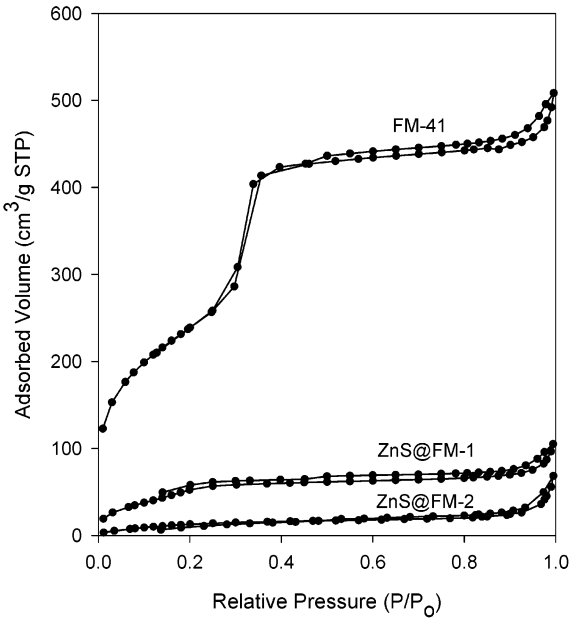

Figure 4. Nitrogen adsorption isotherms for FM-41, ZnS@FM-1, and ZnS@FM-2. The characteristic capillary condensation observed for FM-41 is largely suppressed for the nanocomposites with ZnS NPs. The primary pore volume (V_p) is estimated from the total pore volume after subtraction of the macropore volume that is approximated to the adsorbed volume in the relative pressure range above 0.7.

materials.[6−8,12,14] For the empty FM-41 host, the nitrogen adsorption isotherm shows characteristic capillary condensation around the relative pressure (P/P_0) of 0.33, and the Brunauer−Emmett−Teller (BET) surface area (S_{BET}) and the primary pore volume (V_p) are estimated to be 876.7 m^2/g and 0.76 cm^3/g, respectively (Figure 4). After the first incorporation of the ZnS NPs within the FM-41 host (ZnS@FM-1), the nitrogen adsorption isotherm shows a much suppressed BET surface area (S_{BET} = 213.8 m^2/g) and primary pore volume (V_p = 0.15 cm^3/g), and the characteristic capillary condensation is hardly observed. After further incorporation of the ZnS NPs (ZnS@FM-2), the nitrogen adsorption isotherm shows a BET surface area (S_{BET} = 56.3 m^2/g) and primary pore volume (V_p = 0.03 cm^3/g) more suppressed than those of ZnS@FM-1. Such results also indicate that the loading content of ZnS NPs within the FM-41 host increases with the repetitive insertion.

PL and PLE spectra of the nanocomposites measured at room temperature are shown in Figure 5. Although the PL and PLE spectra of the ZnS NPs confined within the FM-41 host channels include the defective emission of the siliceous FM-41 host itself[27] in a similar spectral range, the emission of the ZnS NPs can be clearly distinguished from the emission of the FM-41 host itself with respect to the differences in the intensities and the spectral positions for the following reasons: The X-ray diffraction data and the TEM images in Figures 2 and 3 suggest that the greater insertion of the ZnS NPs from ZnS@FM-1 to ZnS@FM-2 does not seem to cause any significant perturbations in the pore size and structure of ZnS@FM-2. It implies that the number of defects in the host framework and the involved emission states are similarly preserved in both the ZnS@FM-1 and ZnS@FM-2 cases. Therefore, the enhanced emission intensity of ZnS@FM-2 compared with that of ZnS@FM-1 can be considered to be due to the more confined ZnS NPs existing within the host channels. Furthermore, the inside of FM-41 is modified with the organic thiols and the inserting ZnS NPs are surrounded with AOT molecules. Due to the interface layer of the organic thiols and the AOT molecules between the inserted

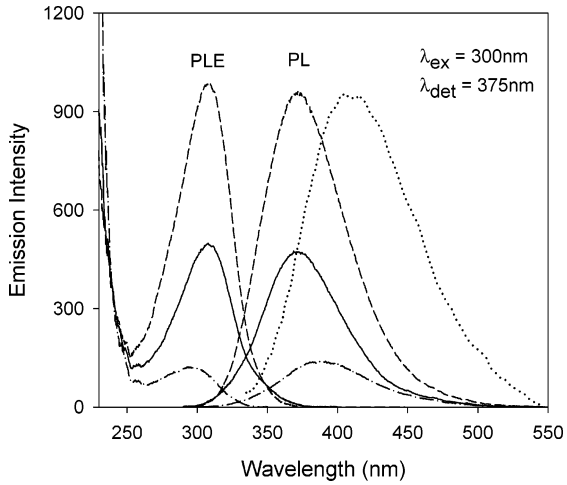

Figure 5. PL and PLE spectra for FM-41 (dashed−dotted line), ZnS@FM-1 (solid line), and ZnS@FM-2 (dashed line) measured at room temperature. Excitation (λ_{ex}) and detection (λ_{det}) wavelengths are 300 and 375 nm, respectively. The emission spectrum of the ZnS NPs in the water pool of reverse micelles (dotted line) is also presented for the comparative study (not to scale).

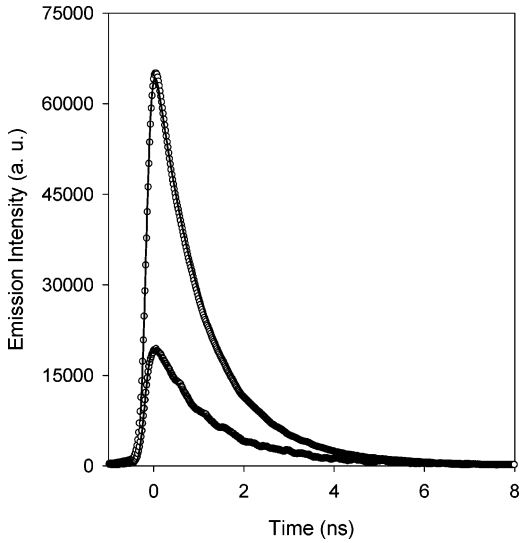

Figure 6. Time-resolved PL decays for ZnS@FM-1 (lower curve) and ZnS@FM-2 (upper curve) measured at room temperature. The emission intensity of ZnS@FM-2 is too high to be compared with that of ZnS@FM-1; therefore, the intensity of ZnS@FM-2 is reduced by a factor of 10. Excitation and detection wavelengths are 290 and 380 nm, respectively. Since the PL decays for the nanocomposites incorporated with ZnS NPs also include lifetime components of 0.4 and 1.0 ns with small amplitudes (less than a total of 20%) due to the FM-41 host itself, the PL decays for the confined ZnS NPs are presented after subtraction of the background PL decay of the FM-41 host itself. The lifetime component only for the confined ZnS NPs was well isolated by a single exponential through the iterative least-squares deconvolution fitting method, and the fitted lines are superimposed on the respective PL decay data (solid line).

ZnS NPs and the framework of the FM-41, the direct coupling between the ZnS NPs and the defective emission states within the host framework does not seem to be enough to change the emission peak of the defective states within the host framework by ∼17 nm (in Figure 5, the emission peaks of 390 and 373 nm are assigned to the FM-41 host and the ZnS@FM-1,2 nanocomposites, respectively).

For the ZnS@FM-1 and ZnS@FM-2 nanocomposites, the PLE spectra centered around 308 nm are red-shifted by ∼0.48 eV from the corresponding absorption spectra centered at 275 nm. These spectral maxima of the red-shifted PLE spectra correspond to the absorption edge of the nanocomposites (inset of Figure 1B). Such red-shifted PLE spectra suggest that the lowest electronic levels of the excited states dominantly contribute to the emissions for the confined ZnS NPs.

Previously, colloidal ZnS NPs showed broad emissions ranging from 400 to 600 nm.[23,24] In a recent study, a broad blue emission (centered at 430−450 nm) was also reported for the ZnS NPs in situ generated within mesoporous material.[14] Such largely Stokes shifted blue emissions are believed to originate from the surface defect states, such as sulfur vacancies. These surface defect states are, however, difficult to control due to the complicated coupling nature with the environments.

In this study, a similar broad blue emission is also observed for the ZnS NPs generated in the water pool of reverse micelles. However, contrary to the case of the ZnS NPs in reverse micelles, it is noticeable that the incorporated form of ZnS NPs within the mesoporous FM-41 host does not show any of the broad blue emission originating from the surface defect states, but presents a new ultraviolet emission centered at ∼373 nm with a Stokes shift of ∼0.7 eV from the corresponding PLE spectra (308 nm). The PL intensity is further enhanced with the increased loading amount of the ZnS nanoparticles (Figure 5). In a colloidal ZnS semiconductor, the photoexcited carriers (electrons and holes) typically recombine with each other through various recombination paths such as direct band-to-band recombination, shallowly trapped recombination via lattice vacancies, and deeply trapped recombination via surface vacancies. Along with the various recombination processes, an emission with a Stokes shift of 0.67 eV[28] and a trap depth of 0.75 eV[29,30] were also observed for the previous study of the colloidal ZnS particles, and were assigned to the emission from the shallowly trapped recombination through lattice sulfur vacancies. Since such an emission has a Stokes shift and a trap depth well-correlated with those of the emission for the confined ZnS NPs within the FM-41, the newly observed ultraviolet emission is, therefore, considered to be from the recombination process at the core lattice sulfur vacancy, not the surface sulfur vacancy, states. Additionally, since the observed emission band from the confined ZnS NPs within the FM-41 host channels has a spectral range of 300−500 nm, it is also possible that the band-edge emission[26,31] can be a contributing factor to the emission edge at a shorter wavelength of 300−330 nm, which is expected from the estimated quantum size (2.0−2.2 nm in diameter) of the confined ZnS NPs. Such observed emission control of reducing the surface states of the ZnS NPs was accomplished by capping of the surface sulfur vacancies with the organic thiols introduced onto the inside surface wall of the FM-41 nanochannels: the particle size of the utilized ZnS NPs (2.0−2.2 nm in diameter) is almost exactly the same as the inside diameter of the thiol-functionalized FM-41 nanochannel (2.0−2.4 nm[16,18]).

ZnS NPs usually present multicomponent PL lifetimes ranging from picoseconds to microseconds.[19,32,33] Such complicated PL decays might be responsible for the complicated interactions of a variety of defect states existing in the ZnS NPs with their environments. Figure 6 shows the time-resolved PL decays for the nanocomposites including ZnS NPs, and both of them present similar PL decay rates regardless of their loading levels. It is noteworthy that the observed PL decays for the incorporated ZnS NPs can be reasonably fitted to a single-exponential decay with a time constant of 1.3 ± 0.2 ns, contrary to the previous results of multicomponent PL lifetimes.[19,32,33] This lifetime reflects the photoexcited carrier recombination rate through the core lattice sulfur vacancies existing in the confined

ZnS NPs within the FM-41 host pore channel. Furthermore, the single recombination lifetime implies that the newly observed ultraviolet emission results from highly selective emission states.

4. Conclusions

In summary, ZnS NPs were highly loaded within well-ordered nanochannels, which was accomplished by repetitive insertion of the guest ZnS in reverse micelles into an organic thiol-functionalized mesoporous host. The ultraviolet emission of 1.3 $\pm$ 0.2 ns lifetime is only observed for the nanocomposites containing ZnS NPs, which is considered to dominantly originate from the potential traps of core lattice sulfur vacancies existing in the confined ZnS. Such a selective ultraviolet emission resulting from structural confinement of the ZnS NPs within the functionalized mesoporous host provides new potentials for their applications as ultraviolet optical devices.

Acknowledgment. This work was financially supported by a National Research Laboratory (Grant No. M1-0302-00-0027) program, the National R&D Project for Nano-Science and Technology (Grant No. M1-0214-00-0021), and a grant from KOSEF (R01-1999-000-00039-0). We are grateful for instrumental support from the equipment facility of CRM-KOSEF. D.-J.J. thanks the Strategic National R & D Program (M1-0214-00-0108).

References and Notes

(1) Shin, H. J.; Ryoo, R.; Liu, Z.; Terasaki, O. *J. Am. Chem. Soc*. **2001**, *123*, 1246.

(2) Kang, H.; Jun, Y.; Park, J.-I.; Lee, K.-B.; Cheon, J. *Chem. Mater*. **2000**, *12*, 3530.

(3) Fukuoka, A.; Araki, H.; Sakamoto, Y.; Sugimoto, N.; Tsukada, H.; Kumai, Y.; Akimoto, Y.; Ichikawa, M. *Nano Lett*. **2002**, *2*, 793.

(4) Jung, J.-S.; Chae, W.-S.; McIntyre, R. A.; Seip, C. T.; Wiley, J. B.; O′Connor, C. J. *Mater. Res. Bull*. **1999**, *34*, 1353.

(5) Srdanov, V. I.; Alxneit, I.; Stucky, G. D.; Reaves, D. M.; DenBaars, S. P. *J. Phys. Chem. B* **1998**, *102*, 3341.

(6) Agger, J. R.; Anderson, M. W.; Pemble, M. E.; Terasaki, O.; Nozue, Y. *J. Phys. Chem. B* **1998**, *102*, 3345.

(7) Winkler, H.; Birkner, A.; Hagen, V.; Wolf, I.; Schmechel, R.; Seggern, H.; Fischer, R. A. *Adv. Mater*. **1999**, *11*, 1444.

(8) Parala, H.; Winkler, H.; Kolbe, M.; Wohlfart, A.; Fischer, R. A.; Schmechel, R.; Seggern, H. *Adv. Mater*. **2000**, *12*, 1050.

(9) Zhang, Z.; Dai, S.; Fan, X.; Blom, D. A.; Pennycook, S. J.; Wei, Y. *J. Phys. Chem. B* **2001**, *105*, 6755.

(10) Chae, W.-S.; Hwang, I.-W.; Jung, J.-S.; Kim, Y.-R. *Chem. Phys. Lett*. **2001**, *341*, 279.

(11) Chae, W.-S.; Kim, Y.-R.; Jung, J.-S. *J. Phys. Chem. B* **2003**, *107*, 1585.

(12) Brieler, F. J.; Fröba, M.; Chen, L.; Klar, P. J.; Heimbrodt, W.; Nidda, H.-A. K.; Loidl, A. *Chem.—Eur. J*. **2002**, *8*, 185.

(13) Kageyama, K.; Tamazawa, J.-I.; Aida, T. *Science* **1999**, *285*, 2113.

(14) Zhang, W.-H.; Shi, J.-L.; Chen, H.-R.; Hua, Z.-L.; Yan, D.-S. *Chem. Mater*. **2001**, *13*, 648.

(15) Besson, S.; Gacoin, T.; Ricolleau, C.; Jacquiod, C.; Boilot, J.-P. *Nano Lett*. **2002**, *2*, 409.

(16) Xu, W.; Liao, Y.; Akins, D. L. *J. Phys. Chem. B* **2002**, *106*, 11127.

(17) Chae, W.-S.; Ko, J.-H.; Hwang, I.-W.; Kim, Y.-R. *Chem. Phys. Lett*. **2002**, *365*, 49.

(18) Hirai, T.; Okubo, H.; Komasawa, I. *J. Phys. Chem. B* **1999**, *103*, 4228.

(19) Chung, J. H.; Ah, C. S.; Jang, D.-J. *J. Phys. Chem. B* **2001**, *105*, 4128.

(20) Rossetti, R.; Hull, R.; Gibson, J. M.; Brus, L. E. *J. Chem. Phys*. **1985**, *82*, 552.

(21) Nanda, J.; Sapra, S.; Sarma, D. D.; Chandrasekharan, N.; Hodes, G. *Chem. Mater*. **2000**, *12*, 1018.

(22) Lippens, P. E.; Lannoo, M. *Phys. Rev. B* **1989**, *39*, 10935.

(23) Becker, W. G.; Bard, A. J. *J. Phys. Chem*. **1983**, *87*, 4888.

(24) Chen, W.; Wang, Z.; Lin, Z.; Lin, L. *J. Appl. Phys*. **1997**, *82*, 3111.

(25) Vossmeyer, T.; Katasikas, L.; Giersig, M.; Popovic, I. G.; Diesner, K.; Chemseddine, A.; Eychmüller, A.; Weller, H. *J. Phys. Chem*. **1994**, *98*, 7665.

(26) Sooklal, K.; Cullum, B. S.; Angel, S. M.; Murphy, C. J. *J. Phys. Chem*. **1996**, *100*, 4551.

(27) Gimon-Kinsel, M. E.; Groothuis, K.; Balkus, K. J. *Microporous Mesoporous Mater*. **1998**, *20*, 67.

(28) Li, Y.; Ding, Y.; Zhang, Y.; Qian, Y. *J. Phys. Chem. Solids* **1999**, *60*, 13.

(29) Chen, R.; Kirsh, Y. *Analysis of Thermally Stimulated Processes*; Pergamon: Oxford, 1981.

(30) Chen, W.; Wang, Z. G.; Lin, Z. J.; Lin, L. Y. *Appl. Phys. Lett*. **1997**, *70*, 1465.

(31) Wageh, S.; Shu-Man, L.; You, F. T.; Xu-Rong, X. *J. Lumin*. **2003**, *102−103*, 768.

(32) Khosravi, A. A.; Kundu, M.; Jatwa, L.; Deshpande, S. K.; Bhagwat, U. A.; Sastry, M.; Kulkarni, S. K. *Appl. Phys. Lett*. **1995**, *67*, 2702.

(33) Smith, B. A.; Zhang, J. Z.; Joly, A.; Liu, J. *Phys. Rev. B* **2000**, *62*, 2021.